Journal of Asian Earth Sciences 206 (2021) 104626

Contents lists available at ScienceDirect

Journal of Asian Earth Sciences

journal homepage: www.elsevier.com/locate/jseaes

Late Pleistocene sea-level changes and the formation and fill of bent valleys incised into the shelf of the western South China Sea

Andreas Wetzel [a,*], Agata Feldens [b], Daniel Unverricht [c], Karl Stattegger [c,d], Rik Tjallingii [e]

[a] Geologisch-Paläontologisches Institut, Universität Basel, Bernoullistrasse 32, CH-4056 Basel, Switzerland
[b] Leibniz Institute for Baltic Sea Research Warnemünde, 18119 Rostock, Germany
[c] Institut für Geowissenschaften, Christian-Albrechts-Universität, Otto-Hahn-Platz 1, D-24118 Kiel, Germany
[d] Geohazards Lab, Institute of Geology, Adam Mickiewicz University, Bogumiła Krygowskiego 12, PL-61-680 Poznań, Poland
[e] Geoforschungszentrum, Telegrafenberg, D-14473 Potsdam, Germany

ARTICLE INFO

Keywords:
Mekong River
Red River
Sea-level change
Incised valley
Meander

ABSTRACT

During times of lowered sea level, Mekong River and Red River incised valleys into the ancient coastal plains of the exposed shelves of the western South China Sea. The deglacial fill history of the incised valley was investigated by seismic surveys and sediment cores. The channels mainly exhibit a low-sinuosity course, but some channel segments are bent. The oldest part of the channel-bend fill exhibits shingled reflectors in Parasound seismic records documenting lateral channel migration typical of meandering rivers. Above, vertically stacked reflectors, which extend from the inner-bend side onto the cut-bank side document that the river-mouth channel turned to a mainly depositional mode. Vertical aggradation started when sea level was ~ 1–2 m below river water-level. During this phase, about two-third of the channel depth was filled by "fluvial-to-estuarine" mud having negative log(Ti/Ca) values as evidenced in XRF core scan data. Typically estuarine conditions developed when river water-level was approximate to sea level. Today channel bends form in estuaries within the zone of bedload convergence. Therefore, it is suggested that the studied channel bends represent antecedent, inherited features that formed during phases of prolonged phases of lowered, but relatively stable sea level to allow bends morphologically to develop. In fact, the bends occur not only in the western South China Sea but also in other areas of the world within a depth range that corresponds to times of retarded sea-level fall during MIS 5b, 5d, 4, and 3.

1. Introduction

Incised valleys and their fills represent condensed archives of the complex sedimentologic and stratigraphic development of coastal regions during transgression whereas adjacent shelf areas often store an incomplete sediment record because of physical reworking of the deposits (e.g., Mattheus and Rodriguez, 2011). Commonly incised-valley systems form during lowering of the base level due to a relative sea-level fall that is marked by an abrupt seaward shift of coastal facies and an associated development of a sequence boundary (Zaitlin et al., 1994). The time span during that a specific incised-valley system develops and becomes filled depends on the interplay of various factors, such as fluvial discharge, erosion vs. deposition of sediment, influence of tides, rate of base-level/sea-level change, duration of lowered base level etc. (for a review see Boyd et al., 2006; Blum et al., 2013; Wang et al., 2019). Besides economic aspects, such as enrichment of sand representing reservoirs or aquifers (e.g., Boyd et al., 2006), incised valleys store information about local as well as global environmental changes like uplift within foreland basins (e.g., Plint and Wadsworth, 2006), glacier dynamics (Fraser, 1994), or sea-level changes (e.g., van Wagoner et al., 1988).

During the Pleistocene, high-frequency high-amplitude sea-level changes led to incision of valleys by rivers traversing the exposed shelves when the sea level was lowered (e.g., Schumm, 1981; Emery and Myers, 1996). In response to falling sea-level, a river traversing a cohesive substrate incises backward to approach a new equilibrium, which starts from the actual base level at the river mouth (e.g., Schumm, 1993). The rates of sea-level fall during Pleistocene glaciations were much more rapid than backward incision and thus, rivers remained in geomorphic disequilibrium and hence, in a potentially erosional mode

* Corresponding author.
E-mail address: andreas.wetzel@unibas.ch (A. Wetzel).

https://doi.org/10.1016/j.jseaes.2020.104626
Received 26 June 2020; Received in revised form 2 October 2020; Accepted 12 November 2020
Available online 23 November 2020

(e.g., Schumm, 1993; Fagherazzi et al., 2004; Loget and van den Driessche, 2009). The sea-level records of the subsequent transgression can be extracted from incised-valley fills, as, for instance, convincingly demonstrated for the Holocene by Tjallingii et al. (2010, 2014). Obviously, only the sea-level rise is well preserved, whereas the temporal record of sea-level fall is poorly documented on clastic shelves because the coastline migrates further seaward and the exposed coastal plains are subjected to erosion as rivers incise deeper. If the sea level resides for some time in a similar position, characteristic geomorphologic features can be formed by the rivers, for instance, meanders (e.g., Miall, 2010; Blum et al., 2013). Concerning the last glacial cycle, the time period of the formation of incised valleys during sea-level fall was much longer than the period for filling up the valleys during deglacial sea-level rise.

The formation of channel bends close to the mouth of a river incising a valley into the coastal plain has been outlined, for instance, by van Wagoner et al. (1990). Recently, such features are increasingly addressed and described in literature (e.g., Weber et al., 2004; Menier et al., 2006; Simms et al., 2006; Reijenstein et al., 2011; Miall, 2011). Except the statement of the similarity with fluvial point bars, the fills of such bends and the involved processes have not been investigated in detail yet to our knowledge. In turn, the environmental significance of incised-valley bends is not well known. Their depositional setting, however, can be deduced from fill architecture in combination with facies analysis.

On different shelf areas of SE Asia, filled bent incised-valley segments have been discovered (Sathiamurthy and Rahman, 2017, and references therein). Furthermore on low-gradient shelf areas like those bordering the western South China Sea, the incised-valley fill records well effects of sea-level changes (e.g., Wetzel et al., 2017). The channel-fill deposits are geometrically similar and exhibit characteristic packages of genetically related reflectors (Bui et al., 2013). Such sediments occur in different regions and water depths and hence, do not represent singular cases rather than recurrently developed features.

It is the purpose of this study to describe the fill architecture of incised-valley bends in the Gulf of Tonkin and off southern Vietnam, to interpret their formation and fill history and to outline their sedimentologic and stratigraphic significance in a generalized conceptual model.

2. Study area and geological setting

The South China Sea is surrounded by the Southeast Asian mainland in the north and west and the islands of Borneo, Palawan, Luzon and Taiwan to the south and east (Fig. 1). It includes large shelf regions, in particular the Gulf of Tonkin in the NW and the Sunda Shelf in the SW that extends from the southern Vietnam coast including the Mekong River Delta to the Indonesian archipelago. These two shelf areas were studied in detail with respect to the incised-valley fill architecture of the ancient Mekong River and Red River (Fig. 1).

The entire region of the South China Sea is influenced by the monsoon system (e.g., Tomczak and Godfrey, 1994). Two different regimes of monsoonal circulation affected the South China Sea during Quaternary (e.g., Wang et al., 1999, Wang and Li, 2009). *Interglacial times* as today are characterized during winter (November to March) by weak seasonality and NE-monsoon that originates from large Siberian high-pressure cells and results in a dry season, whereas during May to September, the SW-monsoon provides humidity and leads to the wet season in the SE-Asian mainland (Wang et al., 1999; Wang and Li, 2009). *Glacial times* are characterized by strong winter monsoon and weak summer monsoon and low wetness in subtropical China (e.g., Wang et al., 1999; Liu et al., 2007). Therefore, fluvial runoff to the northern part of the South China Sea decreased, whereas the discharges of the Mekong River and other rivers flowing into the western part of the South China Sea increased significantly because their catchment areas are located further to the west (Wang et al., 1999). During glacial times, when sea level was lowered by 130 to 120 m (e.g., Hanebuth et al., 2009), wide shelf areas were exposed and were drained by several rivers,

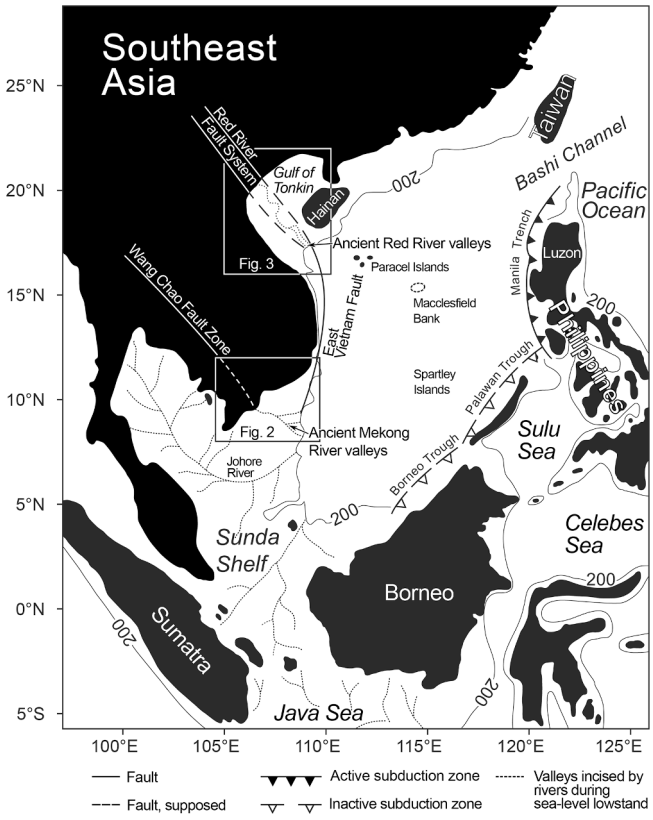

Fig. 1. South China Sea and adjacent areas. Boxes indicate areas studied in detail, the area offshore the present-day Mekong River delta (Fig. 2) and the Gulf of Tonkin (Fig. 3). 200 m water depth isobaths is marked. Major tectonic elements after Clift et al. (2008) and Fyhn and Phach (2015).

that is a shelf width of 250 km for the continuation of the Mekong River and 500 km for the Red River (e.g., Voris, 2000).

After the last glacial maximum, inundation of the exposed shelf areas started around 19.6 ka ago (Hanebuth et al., 2009) and continued until the mid-Holocene sea-level highstand at ~ 6 ka (Stattegger et al., 2013). Sea-level rise and the concomitant rise of local base level resulted in fluvial aggradation in the incised valleys and transformed them into estuaries during ongoing flooding (e.g., Hanebuth and Stattegger, 2003; Tjallingii et al., 2010; Wetzel et al., 2017). The low shelf-gradient allowed for a rapid shift of shorelines and only thin, transgressive shoreface sediments accumulated outside the incised valleys; above a relatively sharp boundary, Holocene marine deposits rest on Pleistocene deposits (e.g., Schimanski and Stattegger, 2005; Tjallingii et al., 2010; Szczuciński et al., 2013). Locally, relict sediments may occur offshore the Mekong River delta (e.g., Jagodziński et al. 2020) and in the Gulf of Tonkin (e.g., Niino and Emery, 1961; Coleman, 1969).

The modern Mekong River Delta covers the region between Phnom Penh in the Cambodian lowlands, the Saigon River mouth, and the southeast Vietnamese coastline (Tanabe et al., 2003; Figs. 1, 2). Today the Mekong River splits in the Cambodian lowlands into the southern Bassac River and the northern Mekong River that diverges in multiple branches turning east- to southeastward further downstream. The lower reaches are nearly straight. The main river-mouth channels are 5 to 10 m deep (Wolanski et al., 1996; Nguyen et al., 2008; Gugliotta et al., 2017). The position and morphology of the Bassac River are tectonically controlled by the NW-SE trending Wang Chao strike-slip fault system (Fig. 1; Morley, 2002). Holocene sedimentation, however, is only little affected by tectonic movements (Ma et al., 2004). The shelf in front of the Mekong River Delta is slightly inclined; along a transect at ~ 10° N, < 0.35 m km^{-1} near the coast and somewhat steeper towards the shelf edge (Fig. 2).

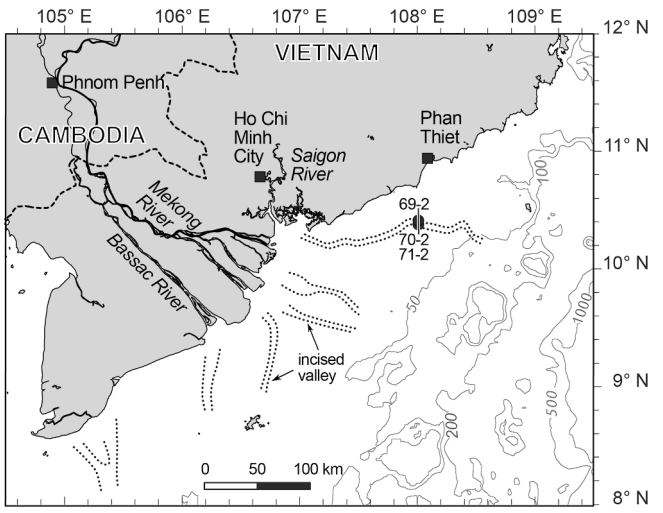

Fig. 2. Map of the area offshore the present-day Mekong River Delta; stippled lines represent boundaries of (so far recognized) valleys that were incised into the exposed coastal plain during the last sea-level lowstand; coring sites are marked by dots and numbers as listed in cruise report of *Sonne* cruise 187 (Wiesner et al., 2006). Line at sites 69, 70, and 71 indicates the seismic record shown in Fig. 4A, C.

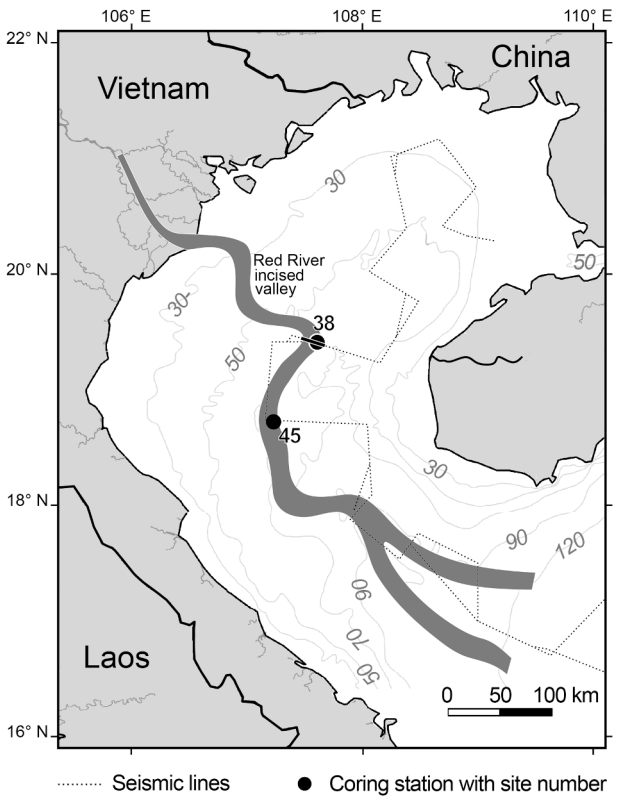

Fig. 3. Gulf of Tonkin; shaded area within the Gulf represents the (so far recognized) valley that was incised into the exposed coastal plain during the last sea-level lowstand; coring site is marked by dot and number as listed in cruise report of *Sonne* cruise 220 (Wiesner et al., 2012). Seismic section across the valley follows ship track. Line at site 38 indicates the seismic record shown in Fig. 4B, D.

Today the southern part of the Mekong River Delta is affected by semidiurnal tides with mean ranges of 2.1 to 2.8 m and up to 4 m during spring-tide conditions (Nguyen, 2012). At the Bassac River mouth, the mean maximum tidal range is 3.2 m, which decreases upstream; tidal effects can reach up to 200 km inland and salt water may flow > 50 km upstream during dry season when river discharge is low (Wolanski et al., 1996; Nguyen et al., 2008; Tamura et al., 2009).

Prior to the 1990′s, the annual discharge of the Mekong River was about 470 km^3 yr^{-1} and the suspended load about 160 Mt yr^{-1} (Milliman and Meade, 1983). During the last decades, however, the suspended river load decreased to 40 Mt yr^{-1} due to upstream dam construction (Binh et al., 2020). The river load fluctuates widely in response to monsoon rainfall, about 80% of the annual discharge occur during summer monsoon (Lu and Siew, 2006).

During times of lowered sea level, the northern branches of the Mekong River flowed further to the east into the South China Sea via numerous incised valleys (e.g., Tjallingii et al., 2010). Incision of the river branches accentuated the Pleistocene landscape as the channels cut down as deep as 30 m. Incision might have been even deeper, because considerable erosion occurred during Holocene transgression (Tjallingii et al., 2010).

The Gulf of Tonkin occupies an area of ~ 90,000 km^2; it is bordered by the island of Hainan in the east and the Asian mainland to the north and the west. The bathymetry of the Gulf of Tonkin is affected by the still active Red River fault system that transverses the gulf (Fig. 1; Gong et al., 2011). The seafloor of the Gulf of Tonkin is covered mainly by siliciclastic muddy sediments, but locally sand and gravel have been encountered and, occasionally, Cenozoic bedrocks crop out (Niino and Emery, 1961). The Gulf of Tonkin experiences a diurnal tidal regime. The tidal range reaches 4 m in the north and 2 m in the south (van Maren, 2007).

The Red River splits east of Hanoi into several distributary channels and forms a lobate delta south of Haiphong before it enters the Gulf of Tonkin (Fig. 3). The river carries about 123 Mt yr^{-1} suspended load and 10 Mt yr^{-1} bed load (e.g., Mathers and Zalasiewicz, 1999; Borges and Huh, 2007). The mean annual discharge is about 3810 m^3 s^{-1} (=120 km^3 yr^{-1}; Mathers and Zalasiewicz, 1999). The discharge fluctuates between 23,000 m^3 s^{-1} and 700 m^{3}s^{-1} during wet and dry season, respectively; about 90% of the annual suspended sediment load is carried during the summer monsoon season (Mathers and Zalasiewicz, 1999). The Holocene architecture of the Red River Delta has been studied in some detail (Tanabe et al., 2006; Funabaki et al., 2007; Hoekstra and van Weering, 2007, and papers therein). Although during glacial times the discharge of the Red River significantly decreased, a well-developed valley was incised (Wetzel et al., 2017). Along that valley, the seafloor mainly exhibits a nearly constant gradient of 0.2 m km^{-1} (Wetzel et al., 2017).

3. Material and methods

Seismic data and cores were collected during cruises 187 and 220 of the German research vessel *Sonne* in 2006 and 2012 to the South China Sea (Wiesner et al., 2006, 2012). The present study is based on several hundreds of kilometres shallow-seismic records crossing incised river valleys and 16, up to 10-m long, 12-cm diameter gravity cores taken along the seismic sections across the incised valleys; two seismic sections and 3 sediment cores retrieved from these transects were selected for a detailed analysis (Figs. 2, 3).

Seismic data were acquired by the Atlas Electronic GmbH Parasound system; the acoustic source as described by Dung et al. (2013) is a hull-mounted device that combines a narrow-beam echosounder and a sub-bottom profiler (e.g., Grant and Schreiber, 1990). The system is operated with a fixed primary frequency of 18 kHz and a secondary primary frequency that varies from 20.5 to 23.5 kHz. Frequency band-pass filters of 2.5 kHz were applied. The data were digitally supplied by the ship's global positioning system (GPS).

The thickness of incised-valley fill-deposits and the vertical extent of sediment bodies were calculated from Parasound data. For seawater a sound velocity of 1475 m/s was determined from CTD measurements. Sound velocity of sediments was assumed to be in the order of 1650 m/s

as measured in marine sediments having similar composition and porosity (Wetzel et al., 1990).

Descriptions of all cores are based on onboard visual observations, digital camera images, and radiographs. For the X-ray radiography, about 1 cm thick sediment slabs were taken from the split core surface directly after opening and sealed to prevent desiccation (Werner, 1967). The slabs were irradiated at the Radiology Centre of the Kiel Medical Care Centre Prüner Gang (Germany) using a Swissray ddR Multi System operated at 40 kV and 100 mAs and automatically controlled radiation time.

High-resolution elemental composition records were measured directly on the split-core surface in a non-destructive way with an Avaatech XRF Core Scanner as described by Tjallingii et al. (2010). After careful cleaning and preparation of the core surface with SPEXCerti Ultralene® foil, *Sonne* 187 and *Sonne* 220 cores were measured with a sample resolution of 2 cm and 1 cm, respectively. This foil avoids both contamination of the instrument sensor and desiccation of the core during the measurements. X-ray fluorescence (XRF) scanner measurements were conducted with a sample time of 30 s and a generator setting of 10 kV (30 kV), which covers the elements Aluminum through to Iron (Lead). More technical details related to the XRF core scanner and sample preparation can be found in Richter et al. (2006) and Tjallingii (2007). To eliminate effects of sediment physical properties, sample geometry etc. on the measured data, the ratios or logarithmic-ratios of two elements were calculated that then can be directly interpreted as the relative concentrations of two elements (Weltje and Tjallingii, 2008). When the log(Ti/Ca) data were determined some time ago, acquisition of replicate measurements was not yet part of the standard XRF core-scanning measurement protocol. Therefore, it is not possible to provide the measurements confidence such as the standard deviation for the log(Ca/Ti) records. However, the obvious signal of the log(Ca/Ti) records suggests a good significance for both elements.

4. Results and interpretation

4.1. Seismic records

Within the extent seismic records obtained from the shelf areas off the Mekong River Delta and within the Gulf of Tonkin, a few transects cross the incised valleys of both, Mekong River and Red River and exhibit a remarkable pattern that resembles the fill structure of meandering rivers (Fig. 4A, B). The valley-fill deposits show a pronounced asymmetry in cross-section having a gentle slope on one side and a steep margin on the opposite side (Fig. 4). Although the cross-section of the ancient Mekong River incised valley appears roughly symmetrical, the fill sediments display marked asymmetry (Fig. 4A, C). The measurements of these valley segments are given for the cross-sections at site 69 of the ancient Mekong River (M) and at site 38 for the ancient Red River (R) (see Figs. 2, 3). The channels are 2 to 3 km wide and their fill is about 23 m (M) and 10 m (R) thick. The deglacial valley fill that is studied here in detail is bound at the base by a locally not sharp, sometimes irregularly shaped reflector that continues into the steep valley margin. In these cases, the base of the deglacial fill is at ~ –68 (M) and –78 m (R) below sea level (BSL), respectively. The deposits resting on this reflector represent the deglacial valley fill. The marine transgressive surface is located at –45 m (M) and –65 (R), respectively.

The deglacial valley fill is arranged in 4 packages (I to IV), each of them characterized by a uniform arrangement of the reflectors. The packages of reflectors differ in their geometry and they are separated either by more or less prominent high-amplitude reflectors or by a subtle erosional truncation or by both (Fig. 4C, D).

Package I constituting the lower part of the deglacial fill starts with an interval of not very well organized reflectors that develop into a well-developed bundle of inclined reflectors that are discontinuous, shingled and dip at 1° to 2° towards the steep margin of the valley. Within this package, small-scale discontinuities may occur. The reflectors tend to become flat towards their base and top. The reflectors constituting

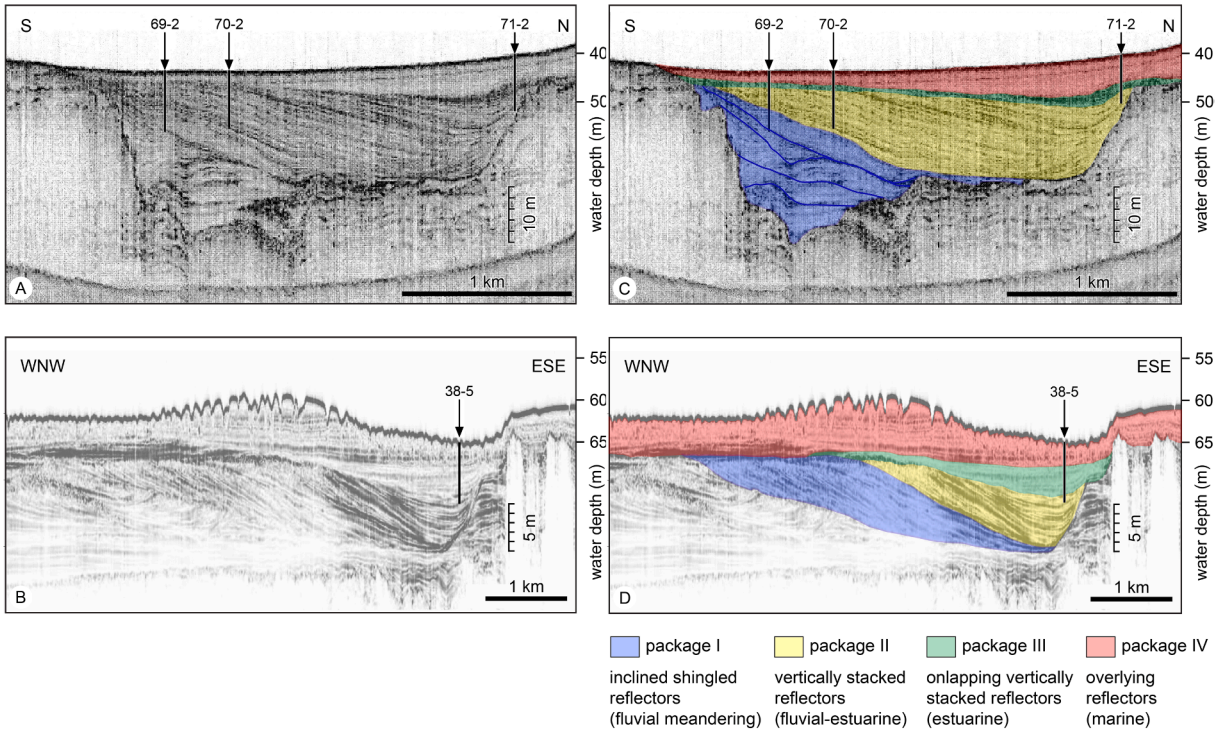

Fig. 4. . Seismic records of the fill architecture of meandering incised-valleys. (A) Seismic record across the valley incised by the Mekong (coring sites 69 and 70; see Fig. 2), (B) seismic record across the valley incised by the Red River (coring site 38; see Fig. 3); (C) seismic record across the valley incised by the Mekong as in (A) with four marked packages of reflectors (coring sites 69 and 70; see Fig. 2), (D) seismic record across the valley incised by the Red River as in (B) with four marked packages of reflectors (coring site 38; see Fig. 3). – Vertical bars at the coring sites indicate core length.

package I show a lateral shift and they have a maximum vertical extent of up to 21 m (M) and 9 m (R). For the transect across the ancient Red River valley that is not affected by pre-existing morphology, package I reflectors show a downward shift. The boundary to the overlying package II is transitional, but the basal reflector of package II and those above onlap onto the steep valley flank in contrast to those of package I.

Package II consists of vertically stacked reflectors, which show a convex-downward shape exhibiting a decreasing curvature upward. This package is in maximum 18 m (M) and 9 m (R) thick, but in the channel axis only 14 m (M) and 5 m (R). The width of the channel decreased during the formation of package II from 2.5 km to 1 km (M) and 2 km to 1 km (R), respectively. During formation of package II the reflectors migrated still gradually outward at the steep valley side by a total of 450 m (M) and 300 m (R), respectively, but the amount of shift decreases upward.

Package III exhibits a conformable contact to package II in the centre of the channel that, however, becomes unconformable towards the gently dipping margin of the channel. Laterally it continues into a slight erosional truncation in contact to package I. Above that, the reflectors of package III onlap onto packages I, II and onto the steep valley margin as well. The boundary between packages II and III exhibits a vertical relief of about 5 m (M) and 3 m (R). The reflectors of package III show a slight vertical stacking. The valley cross-section widens from about 1 km to 2.2 km (M) and 1.9 to 3.4 km (R), respectively. Package III ends laterally and vertically at the valley shoulders and completes the valley infill.

Package IV is characterized by reflectors being roughly parallel to the topography below, inside and outside of the valley. The boundary between package III and IV is often transitional.

4.2. XRF core-scan data and lithofacies

All cores of the incised-valley fill-deposits exhibit a similar pattern of the XRF core-scan data with respect to the log(Ti/Ca) values. The ratio of the elements Titanium (Ti) and Calcium (Ca) records the relative variation of terrigenous and marine constituents. The conservative element Ti is restricted to lithogenic sediments and inert to diagenetic processes (Calvert and Pedersen, 2007). The element Ti resides in Ti-oxides like rutile and anatase (TiO_2) and is enriched in tropical soils such as laterites and bauxites. The element Ca reflects predominantly the abundance of biogenic carbonates ($CaCO_3$) in marine sediments (Arz et al., 1998; Tjallingii, 2007).

The basal part of all cores exhibits fairly constant log(Ti/Ca) values at around zero (Fig. 5). Further up, there is a transition wherein the log (Ti/Ca) values become clearly negative. This occurs in 180–220 cm and 180–200 cm depth, in the cores 69–2 and 70–2 (ancient Mekong River), respectively, and in 180–220 cm depth, in core 38–5 (ancient Red River). At the transition and somewhat below some negative peaks may occur. The upper part of the cores is characterized by roughly uniform log(Ti/Ca) values at around –1.

Within the studied cores, five main lithofacies (LF) can be distinguished (Fig. 6). The boundaries between them are sharp or gradational. The different lithofacies (LF) are related to both log(Ti/Ca) values and seismic records (see below).

Lithofacies 1 – Lag deposits (LF1; Fig. 6A)

Observations. Above a distinct boundary, greenish, grey, slightly muddy coarse-sandy to pebbly material with mud clasts, carbonate and Fe-oxide nodules rests on stiff to hard consolidated, often multicolored mud. The coarse layer is up 60–80 cm thick. Neither stratification nor burrows are visible. The transition to overlying LF2 is fairly sharp.

Interpretation. The coarse interval represents fluvial lag deposits containing remnants of palaeosols (caliche, iron-oxide nodules, hard mud-clasts). The mud clasts were eroded from channel floor/banks. The multicolored stiff mud underneath is interpreted to have been overprinted by pedogenetic processes. The discontinuity at the base represents an erosional unconformity.

Lithofacies 2 – laminated mud (LF2; Fig. 6B).

Observations. This lithofacies is composed of greenish to greyish laminated mud, but sometimes colour may get some brownish-reddish shading. Up to a few mm thick silt and sand laminae occur occasionally as singular layers, as packages separated by mud laminae, or as up to millimetre-thick mud intervals. Conspicuous thin laminae composed of dark plant debris are intercalated at varying spacing. Locally, light-

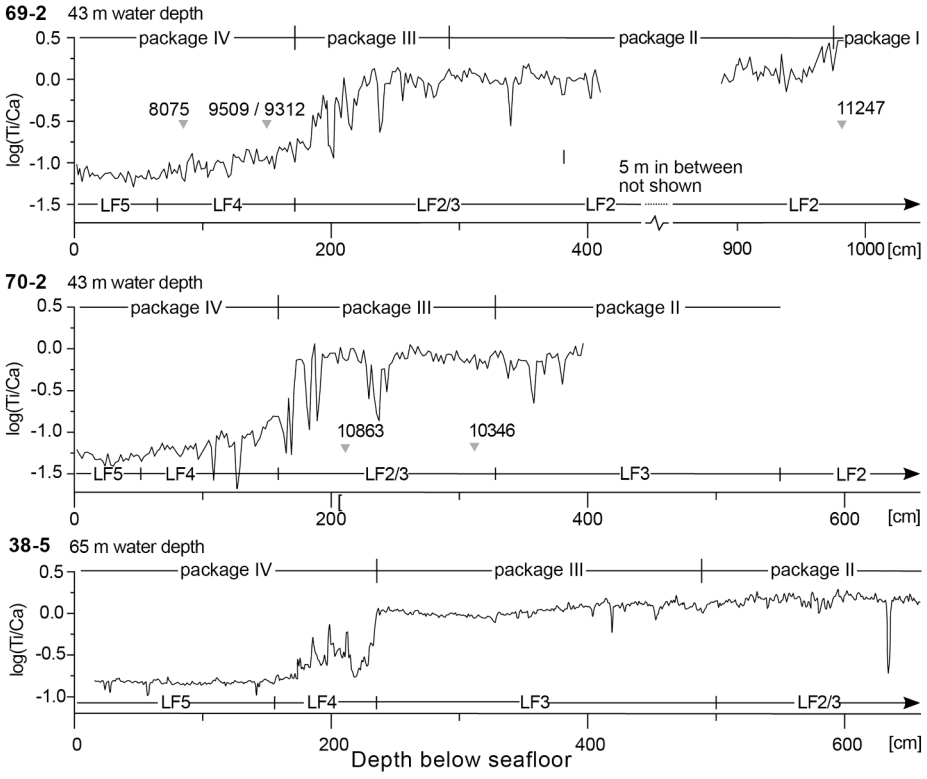

Fig. 5. XRF-scan data of cores taken along a transect crossing an incised valley of the ancient Mekong River (see Figs. 2, 4A) and the ancient Red River (see Figs. 3, 4B). Furthermore, the occurring lithofacies (LF) are shown and the range of the packages of seismic reflectors as shown in Fig. 4C, D. Grey triangles mark age points, the given age is in yr BP (for details of age determination see Tjallingii et al., 2010). Core 69–2 and adjacent core 70–2 were taken at the modern water depth of 43 m, core 38–5 at 64 m.

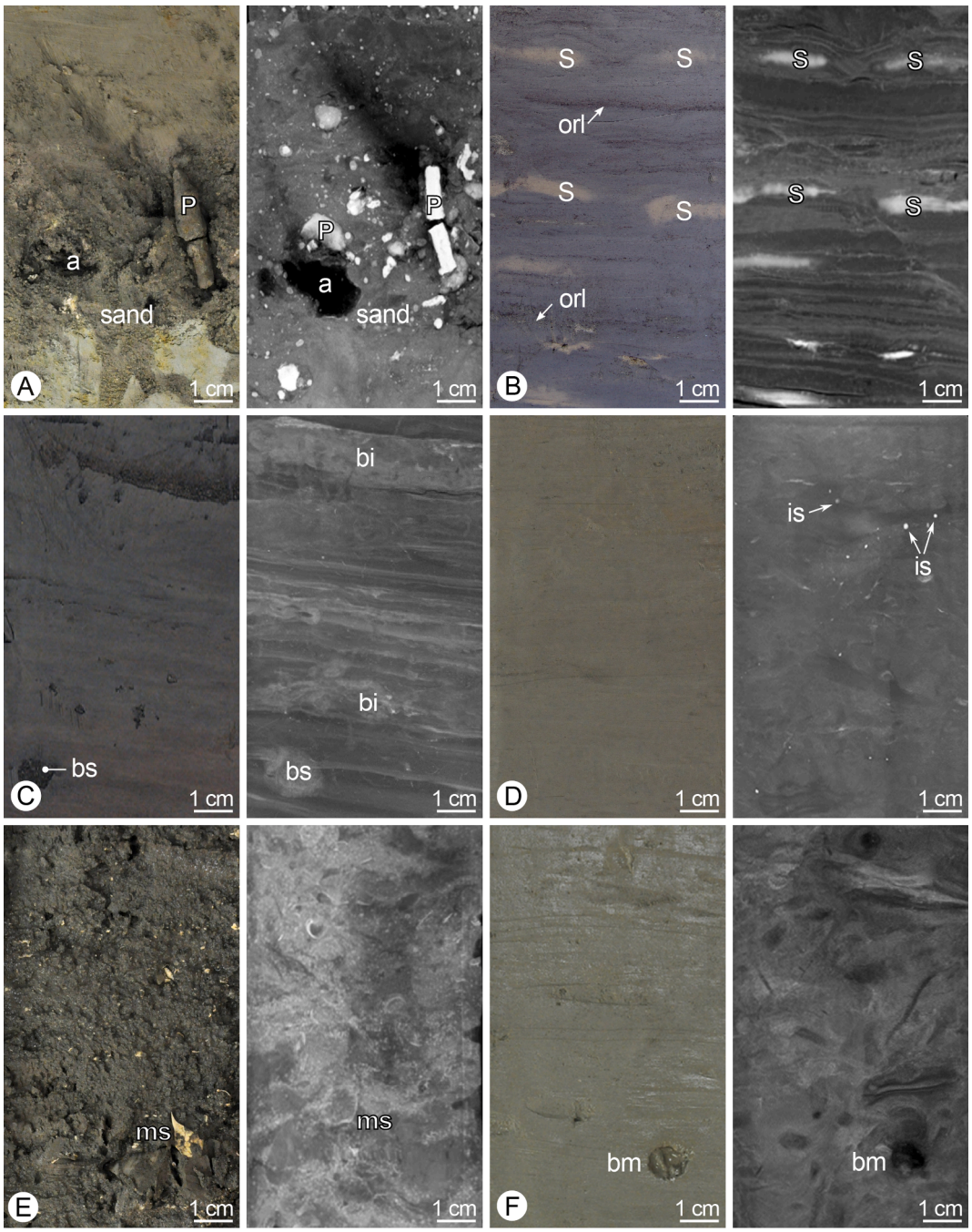

Fig. 6. Examples of lithofacies (LF) encountered at the coring sites, fresh core at the left, X-ray radiograph (negative; sand = light, mud = dark) at the right. (A) LF1 – Fluvial lag deposits consisting of pebbly sand, (a) artefact, pebble lost due to core preparation, (P) pebble (core 45–4, 799–814 cm). (B) LF2 – Laminated fluvial mud; laminae consisting of silt and fine sand are clearly seen in X-ray radiographs, whereas layers rich in organic debris cannot be distinguished; the latter, however, are evident in fresh core (orl); siderite (S) implies pore-water containing a high proportion of freshwater (core 69–2, 869–881 cm). (C) LF 2/3 –Thin alternating intervals consisting of laminated mud (LF2) and bioturbated mud LF3, (bi) intensely bioturbated interval, (bs) sand-filled burrow (core 69–2, 340–355). (D) LF3 – Bioturbated estuarine mud appearing homogeneous in fresh core but exhibits biodeformational structures in X-ray radiography; iron-sulfides (is) imply originally sulfate-rich pore water (core 38–5, 223–238 cm). (E) LF4 – Bioturbated sand deposited just above the marine transgressive surface; originally deposited layers consisting of sand and shell debris (ms) were mixed by burrowing organisms with mud (core 38–5, 173–188 cm). (F) LF5 – Bioturbated marine mud, burrowing organisms extinguished all primary sedimentary structures; (bm) mud-filled burrow (core 38–5, 24–36 cm).

brownish siderite spots occur deeper in core.

Interpretation. LF2 is interpreted as fluvial-dominated mud because of the constant, relatively high log(Ti/Ca) values at around 0, the absence of marine organisms, and very rare burrows. Furthermore, early diagenetic siderite implies pore water having been low in sulfate prior to diagenesis that is typical of freshwater-dominated settings (Mozley, 1989; Curtis and Coleman, 1986).

Lithofacies 3 – Bioturbated mud (LF3; Fig. 6C)

Observations. This lithofacies consists of greyish to greenish mud. In fresh core, it appears commonly homogeneous, but in X-ray radiographs a high degree of bioturbation can be recognized. In addition, in X-ray radiographs Fe-sulfides can be seen. Where overlain by LF4 this lithofacies stiffens towards the top and can be penetrated by distinct tubular burrows of the *Glossifungites* suite (e.g., MacEachern et al., 2009); some

of these burrows are still open, others are filled with material from above (LF 4 or LF5). Locally *Gyrolithes* trace fossils occur (Wetzel et al., 2010).

Interpretation. This lithofacies formed under estuarine conditions when both fluvial runoff and tides interacted. This interpretation is based on the XRF core-scans providing log(Ti/Ca) values around zero, the stratigraphic position below marine LF4, and the absence of (debris of) marine shells except in some *Glossifungites*-suite burrows filled from above. *Gyrolithes* burrows reflect fluctuating salinity in incised valleys that were filling when estuarine circulation was established during Holocene transgression in a mesotidal setting (Wetzel et al., 2010). Furthermore the presence of Fe-sulfides suggests that the pore water contained a non-negligible sulfate content prior to diagenesis implying influence of seawater (e.g., Curtis and Coleman, 1986; Rickard et al., 2007).

Lithofacies 2/3 – Alternations of laminated and bioturbated mud (LF2/3; Fig. 6D)

Observations. Transitions between LF2 and LF3 occur in almost all cores as centimetric alternations of laminated and bioturbated mud layers. The latter become thicker and more frequent upward until LF3 is dominant.

Interpretation. This transitional lithofacies formed when marine water incurred (occasionally far-upstream) due to storms or during seasonal low river discharge (e.g., Carlin et al., 2015). The deposits were bioturbated during such marine episodes (e.g., Dashtgard et al., 2012) when polyhaline conditions established (Wetzel and Unverricht, 2020), whereas the dominance of fluvial conditions is indicated by the laminated mud.

Lithofacies 4 – Mottled sand (LF4; Fig. 6E).

Observations. LF4 is composed of bioturbated, mottled, poorly sorted fine to coarse sand containing a varying amount of millimetric to centimetric (debris of) marine shells and some admixed mud. The sediment colour varies from pale greenish to yellowish depending on the amount of mud present. Burrows might be enriched in coarse or fine grains.

Interpretation. LF4 represents shallow-marine sand because of low log(Ti/Ca) values and the presence of marine fossils. The considerably high sand content of LF4 is typical of transgressive deposits; the coarse grain-size on top of the *Glossifungites* surface that accentuates the boundary to LF3 implies physical reworking.

Lithofacies 5 – Marine mud (LF5; Fig. 6F)

Observations. In fresh core, LF 5 appears as uniform to slightly mottled greenish mud. In X-ray radiographs, it is seen that the sediment is completely bioturbated. Locally, singular or nests of marine mollusc shells occur being millimetres to a few centimetres in size.

Interpretation. LF5 represents marine mud as it shows negative log (Ti/Ca) values, contains (fragmented) marine organisms, and its top forms the present seafloor. In contrast, the incised-valley fill sediments below are composed of lithogenic material low in carbonate as indicated by high log(Ti/Ca) values around zero (Fig. 5). The marine transgressive surface is situated between these two units and shows a pronounced shift in log(Ti/Ca) values. Recurrent negative log(Ti/Ca) peaks below the marine transgressive surface originate from burrows filled with marine material from above.

One core from the ancient Mekong River incised valley (69–2) reached the top of package-I deposits and provided a calibrated radiocarbon age of 11.2 ka at 9 m core depth (Fig. 5). At this site, full-marine conditions established before 9.5 ka in ~ 200 cm core depth (Tjallingii et al., 2010).

5. Discussion

Because the sediment packages representing the valley fill are genetically related to each other, the valley-fill architecture in combination with the lithological data is interpreted in terms of consecutive depositional processes (e.g., Helland-Hansen and Hampson, 2009) and shown in Fig. 7.

The unconformity bounding the deglacial valley fill at the base

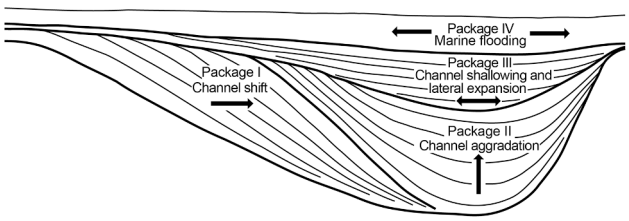

Fig. 7. Schematic subdivision of the incised-valley fill from a fluvial point bar to fully marine sediments. The dimensions of the valley fill may vary horizontally from hundreds of meters to several kilometres and from meters to a few meters in thickness.

continues into the unconformity marking the valley margins (Fig. 4C, D). This unconformity matches only partly the characteristics of a sequence boundary as outlined by Strong and Paola (2008) and Blum et al. (2013); due to lateral shift and widening of the channel, the basal channel surface usually resembles a valley in shape, but it is a highly diachronous, composite feature that never existed as a topographic surface in the subaerial landscape. The lowermost deglacial channel-fill package I comprises inclined and (sub)parallel, more or less continuous, high-amplitude and shingled reflectors. Laterally accreting reflectors are interpreted to represent point-bar deposits that formed by the lateral migration of a meandering channel (e.g., Reijenstein et al., 2011; Janocko et al., 2013). Furthermore, the continuous incision during formation of package I (Fig. 4D) implies a depositional setting above base level and hence, points to a fluvial setting. The encountered LF2 lithofacies supports this interpretation. It contains numerous siderite concretions that in organic-rich estuarine deposits only could form if the pore water is low in sulfate/sulfide otherwise Fe-sulfides would precipitate (Postma, 1982; Mozley, 1989; Curtis and Coleman, 1986). Therefore, siderites in the studied deposits imply strong freshwater influence.

The boundary between package I and II appears to be transitional, but in fact it documents a marked change of the fluvial system, as package II is present on both, the point-bar side and the previous cut-bank side. Therefore, lateral shift of the channel ceased and sediment aggradation started. The vertical accretion pattern strongly suggests that flows have been depositional, even on the cut-bank side. Thus, these channel processes differed from those during point bar formation because the channel switched to an aggrading mode while the cross-sectional area decreased implying a lowering in stream power (e.g., Janocko et al., 2013). Concomitantly lateral channel migration declined. Package II formed within a setting dominated by terrigenous sediments as suggested by the XRF core-scan data. Encountered LF2/3 and LF3 lithofacies, both containing Fe-sulfides, suggest varying marine influence that also induced flocculation of mud in the mixing zone between marine and fluvial waters (e.g., Kineke et al., 1996). Increasing mud aggregation leads to accelerated settling and more rapid deposition (e.g., Portela et al., 2013; Sutherland et al., 2015). Furthermore, tidal effects might have favoured deposition of sediment as flow velocity decelerated during flood and subsequent slackwater (e.g. Dashtgard et al., 2012).

For the marked change in the depositional setting from fluvial (package I) to estuarine (package II) the distance to the shoreline can be estimated. This calculation is based on the geometry of the reflectors of package I, the elevation of the adjacent land surface, and the overall slope of the coastal plain. However, two assumptions are made; (1) the water table in the channel close to the coast was nearly equal to sea level and (2) the uppermost reflector of package I was just covered by water. For the valley incised by the Red River, the top of package I is at –66 m, this is 3 m below the adjacent land surface. As the coastal plain has an overall slope of 0.2 m km^{-1} (see above), the shoreline was about 15 km away. For the ancient Mekong, the adjacent land surface is 6 m above the top of package I and the slope of the coastal plain is 0.35 m km^{-1}.

Thus, the coastline was about 17 km away when the aggrading reflectors started to form. In both instances, 15 km and 17 km from the coast is in the range of the zone affected by seawater and even within the bedload convergence zone of modern rivers (e.g., Dalrymple, 2012; Fig. 8). In case of the modern Fraser River, tidal effects occur up to 90 km upstream, but salt water intrudes only for 30 km during average discharge (e.g., Dashtgard et al., 2012); for the modern Mekong River the corresponding values are 200 km and > 50 km, respectively whereas shells of brackish-water organisms occur as far as 160 km upstream (Gugliotta et al., 2017).

The vertical aggradation pattern is indicative of a rising base level (=sea level). At the time when package I formed, the channel bend was located very likely within the tidal limit as in transgressive-phase estuaries the main channel shows the highest sinuosity within the bedload convergence zone that is located within the upper reach of the tidal limit (e.g., Dalrymple et al., 2012). The onset of marked vertical accretion occurred at ~ 10.8 ka in the cross-section of the ancient Mekong River (Tjallingii et al., 2010, Fig. 6). At that time the sea level was ~ –48 m BSL (Tjallingii et al., 2010, Fig. 7). This is ~ 1 m below the estimated water level in the channel if the upper tip of the shingled reflectors of package I was just covered by water. Therefore, at the onset of the aggradational stage documented by package II, the channel was about 16 m deep (=vertical extent of reflectors of package II) and the rising sea-level modulated sediment aggradation within the channel having its floor ~ 15 m below sea level. Consequently, package II represents the period during that estuarine conditions established. These deposits are ascribed to the late lowstand systems tract.

Package III documents a gradual widening of the channel by reflectors onlapping onto both channel sides suggesting that a funnel-shaped estuary existed. This occurred at an estimated age of 10.2–9.8 ka. At that time, water level within the ancient Mekong River channel (=upper tip of basal reflectors of package III) equalled sea level (~–44 m). The channel was 5.2 m deep as indicated by the vertical extent of package III reflectors. The adjacent land was 1–2 m above sea-level

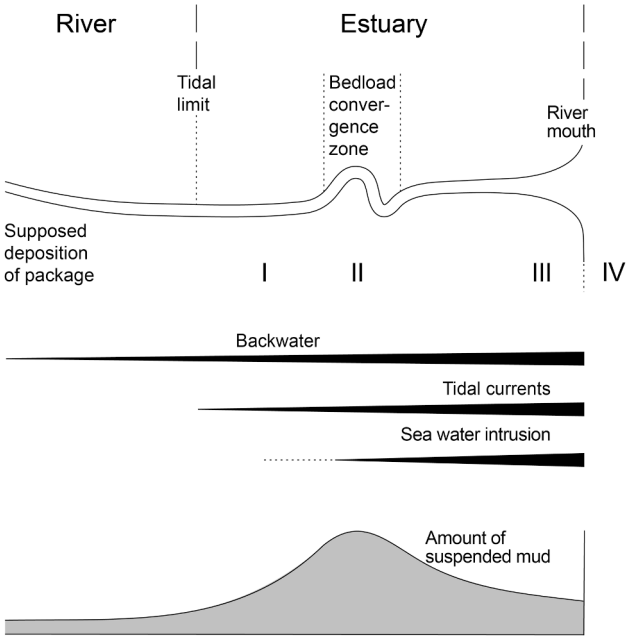

Fig. 8. Scheme showing the various factors active within the lower reaches of a river having an estuary mouth morphology (redrawn from Li, 2006; Dalrymple, 2012, Zhang et al., 2014). The numbers below the line drawing refer to the potential depositional setting of the seismic packages defined in Fig. 7. Because the amount of suspended mud varies considerably due to variations in discharge and seawater intrusion, the graph just represents the relative increase and decrease downstream.

(Fig. 4). The base of package III is slightly erosional because it truncates reflectors of the packages II and even I underneath. The channel was quite shallow, but it expanded and widened upward as indicated by the reflectors onlapping the channel banks. Erosion at the base of the package III points to the interaction of fluvial runoff with tides that increased stream power (e.g., Dalrymple et al., 2012). The reflectors, however, still exhibit a slightly aggrading pattern and hence, indicate further base-level rise. The channel floor moved upward and lateral expansion of the channel enlarged the hydraulic cross-section because of increasing tidal influence (cf. Dalrymple et al., 2012). These deposits are interpreted as early transgressive systems tract that records increasing marine influence within an estuary becoming wider in response to transgression. Package III comprises transitional LF2/3 and LF 3 that both show characteristics of a salinity-stressed setting to a varying degree. The low diversity of the burrows in the bioturbated mud supports this deduction (e.g., Gingras et al., 2012; Wetzel et al., 2017). Package III is capped by a fairly well developed high-amplitude reflector. This reflector very likely represents the marine transgressive deposits of LF4 that rests on a stiffened *Glossifungites* interval. This reflector forms the base of package IV that consists of the marine LF4 and LF5. The latter is characterized by topography-parallel homogeneous-appearing, low-amplitude reflections. Consequently, the deposits of package IV comprise the transgressive and highstand systems tracts.

During the Pleistocene glaciations, sea-level dropped at a higher rate than rivers could incise into the coastal plains and hence, the rivers were not in geomorphic equilibrium and had the potential to cut deeper into the substrate (Muto and Swenson, 2005; Blum et al., 2013). In addition, backward incision of rivers was slow compared to Pleistocene sea-level lowering and thus, it took time to re-acquire an equilibrium river profile depending on the amount of sea-level fall, the resistance of substrate against erosion, stream power etc. (e.g., Bridge, 2003; Mattheus and Rodriguez, 2011). For large river systems, it has been calculated that they respond with a time lag exceeding 100 kyr to short-term base-level fluctuations (Casteltort and van den Driessche, 2003; Clift, 2006; Blum et al., 2013). Therefore, the gradient of large incised valley systems very likely did not reach equilibrium during Pleistocene sea-level falls (e.g., Emery and Myers, 1996; Blum et al., 2013).

During rapid sea-level fall, non-equilibrium conditions very likely prevailed also within the river-mouth region because rivers did not tend to form a delta rather than a simple funnel-like channel that was subsequently incorporated into the incised valley during further sea-level fall (e.g., Hori et al., 2004; Mattheus and Rodriguez, 2011). In spite of the fact that an estuary represents a transitional stage towards a delta being typical of a transgressive setting (e.g., Dalrymple et al., 2012), geometrically similar, funnel-like features might have formed during rapid sea-level fall (cf. van Wagoner et al., 1990; Emery and Myers, 1996).

During rapid sea-level rise, time for geomorphologic equilibration was, again, often too short, in particular in low-gradient coastal plains where little increments in sea-level rise led to far inland shift of the coastline. In this case, the characteristics of modern tide- or wave-dominated estuaries cannot fully develop, for example, cross-bedded sands deposited on elongate estuarine or coastal bars as well as wave-generated structures as typical elements of estuaries (Dalrymple et al., 2012) are absent. Instead, during fast transgression of low-gradient coastal plains the mouth region of an incised valley migrates so rapidly landward that only thin transgressive sand sheets can form within the valleys, in particular, if the rivers are rich in suspended load, as in the studied cases (Wetzel et al., 2017). The resultant thin transgressive sand layers are prone to become completely bioturbated as documented by LF4. Above, the mud-dominated LF5 corresponds to shelf mud accumulating in front or downdrift of modern estuary of a major river that carries large amounts of suspended load (e.g., Unverricht et al., 2014; Zhang et al., 2014). Furthermore, modern estuaries are funnel-shaped and tend to widen exponentially towards the sea. In case of a rapid sea-level change, the widening is very likely less pronounced

because the time to fully develop the funnel shape is too short and the effect of incoming energy such as tides and waves is reduced compared with wide open estuaries that evolved over a few thousands of years (cf. Zhang et al., 2014).

In response to rapid falling base level, rivers first narrow and straighten, then deepen and finally may widen (Schumm, 1981). Accordingly, most seismic records of the valleys incised by the Mekong River and Red River are suggestive of a straight or low-sinuosity channel course that is in accordance with the above scenario (see Figs. 2, 3). Nonetheless, independent of the general fluvial style, a river within an incised valley tends to form meanders near the river mouth (e.g., van Wagoner et al., 1990). Although there is no satisfactory physical explanation for the formation of such channel bends, they are known to occur preferentially upstream the tide-dominated channel segment (Gugliotta and Saito, 2019) or within the zone of bedload convergence where the sediment load is enlarged (Dalrymple et al., 2012). The bedload convergence zone is given by the bedload transferred by tidal currents upstream and fluvial bedload moving downstream (Fig. 8). Modern estuaries, for instance, show characteristic channel bends within the range of the tidal limit (Dalrymple et al., 2012). Evidently, sediment load is an important factor; the more sediment enters a flow the more rapidly are loops developed (Twidale, 2004). For example, various tributaries of the modern Amazon River significantly differ in sediment load and only the rivers carrying a lot of sediment form meanders whereas the others do not (Constantine et al., 2014). Because a channel starts to widen and to migrate when bars are formed (Blum et al., 2013) the large amounts of sediments within the bedload convergence zone and their temporary deposition, for instance, during slackwater may initiate channel migration or avulsion.

The formation of channels bends that are later not subjected to neck cut-off and erosion (Twidale, 2004), lasts considerable time, in the order of a few hundreds of years or more depending on the environmental conditions (e.g., Miall, 1996, 2010). Applying this scenario to the studied cases, the local, but clearly developed channel bends very likely formed during prolonged phases of nearly stable relative sea level. To prove this hypothesis, the water-depth range of the incised valley bends has been compared with the Late Pleistocene sea-level chart according to Waelbroeck et al. (2002). During the last 130 kyr, in particular during MIS 5d, 5b, 4, and 3, there have been periods of prolonged relatively stable or at least little sea-level fluctuations during that the sea-level oscillated recurrently around –45 ± 5 m and –70 ± 5 m BSL (Fig. 9). These depth intervals match fairly well the water-depth range (given by the top of package I) wherein the incised valley bends of the ancient Mekong River and Red River occur (Fig. 4). The Pleistocene sea-level curve, however, is still subject to some degree of uncertainty (e.g., Waelbroeck et al., 2002). The above hypothesis is supported by the observation that channel bends constitute antecedent, inherited forms in coastal plains and affect morphology and drainage pattern (e.g., Phillips and Slattery, 2008). Similarly, the ancient Mekong River valley preserved some palimpsest features (deep channel base underneath the point bar side; Fig. 4A, C) that originated form antecedent forms.

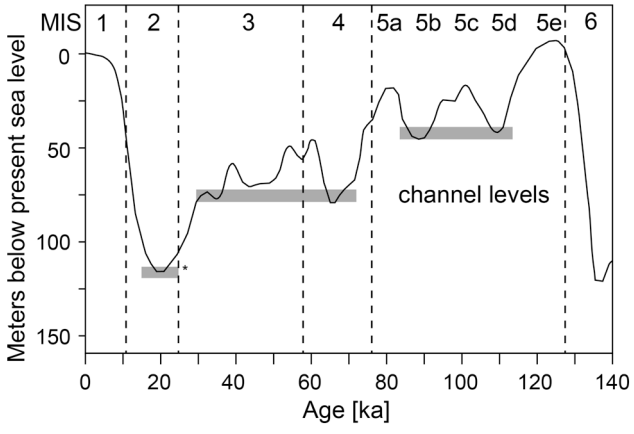

Fig. 9. Sea-level fluctuations for the last Glacial-Interglacial cycle (after Waelbroeck et al., 2002) exhibit a few periods during that the sea-level changed only slowly. During these episodes of retarded sea-level fluctuation, the sea-level was within a depth range that corresponds to the depth of the bent channels (marked with grey bar). * During the last glacial maximum, meanders might have formed close to the corresponding coast line. This coincidence may suggest that then the channel bends formed (for details see text).

If the above hypothesis is valid, also other incised valleys should show such bends in depth ranges that represent episodes of relatively stable sea level. There are some published records of incised valleys having similar fill architecture. On the Sunda Shelf, close to the Malayan peninsula up to 40 m-thick deposits of migrating channels have been found in 70 ± 5 m (Darmadi et al., 2007, fig. 3). The meandering channels shown by Reijenstein et al. (2011) and Alqahtani et al. (2014) in about –95 m depth BSL do not match the above given depth range, but this area is affected by thermal subsidence (Alqahtani et al., 2015) that caused additional deepening and thus, also these meandering channels probably match the above envisaged depth range. For the ancient Charente River offshore France, repeatedly vertical aggrading units have been identified above point bar deposits within bent valleys (Weber et al., 2004, fig. 3A, B, unit U1; Menier et al., 2006, unit U4, fig. 11). The top of the meandering channels is located at –40 ± 2 m BSL. Shingled reflectors within incised valleys have also been described from offshore Texas in a similar water depth by Simms et al. (2006). Similarly, studies addressing the valleys incised by the rivers flowing into the Gulf of Mexico are stated to have widened and shifted during periods of relatively stable, but lowered sea level (Blum et al., 2013, fig. 28). This depth interval matches roughly prolonged phases of relatively stable sea-level that occurred during MIS 2, 3, and 4d (Fig. 9). Filled channel bends have been recognized also in seismic records of the ancient Molengraaff River that drained the Sunda Shelf (Hanebuth et al., 2002, fig. 2a, e). There, the top of the channel fill is located in about –110 to –120 m BSL. This depth is in the range of the sea-level lowstand during the last glacial maximum.

The sedimentary record within Pleistocene incised valleys is definitely biased because continuous incision during falling and low sea level removed very likely parts of the previous deposits. In contrast, during sea-level rise close to the shoreline, the valley is potentially overdeepened because of preceding incision. Consequently, a fluvial system turns into a depositional stage when such a valley segment is affected by rising base level, and the resultant deposits have a high preservation potential. Each shift of a surface expressed in the seismic record across an incised valley, therefore, can be seen as a step within a continuously evolving system and hence, its displacement has sedimentologic significance.

6. Conclusions

1. Bent segments of incised valleys have been observed repeatedly in seismic records of shelf areas bordering the western South China Sea. The Holocene deposits filling incised-valley bends document the change from fluvial over estuarine to marine settings.
2. Above a basal high-amplitude unconformity, (sub)parallel, shingled reflectors document laterally accreted point-bar deposits in a channel of considerable depth. The onset of local base-level rise (=sea-level rise) is given when depositional style changes to vertically stacked aggrading strata. They indicate that the fluvial system turned to a mainly depositional mode and became considerably influenced by seawater and tides. This occurred when the river water-level at the studied sites was ~ 1 m above sea level, but the channel floor was several meters below sea level. The vertical extent of the reflectors provides a measure for channel depth that decreased by about 50% when fluvial-to-estuarine sediments accumulated. The presence of

siderite or iron sulfides in alternating intervals may imply major influence of either fluvial or marine water.

3. At the onset of the following estuarine stage, river water-level was nearly equal to sea level. Increasing influence of tides characterizes the estuarine stage during transgression that led to a roughly twofold widening of channels as documented by onlapping reflectors. Sediment accumulation was low because river runoff and tides interacted. XRF core-scan data in combination with the presence or absence of (fragmented) marine shells, siderite and iron sulfide support the interpretation of an environment changing from fluvial over estuarine to marine.
4. Modern analogues suggest that the channel bends very likely formed within the bedload convergence zone of an estuary during sea-level fall at times of rather stable relative sea level and hence, the bends represent antecedent structures. However, to preserve the bends as antecedent morphological elements during further sea-level lowering they need considerable time to fully develop to escape later destruction. Prolonged periods of relatively stable sea-level occurred during sea-level fall. In fact, channel bends are present in various areas within the depth ranges that correspond to such periods of retarded sea-level fall.

7. Author agreement

All the authors have read the manuscript and agree to submit it for publication to the "Journal of Asian Earth Sciences."

8. Credit author statement

Conception and design of the study (AW), drafting of the manuscript (AW, KS, AS, DU, RT), aquisition of data (AS, DU, RT, KS, AW).

Declaration of Competing Interest

The authors declare that they have no known competing financial interests or personal relationships that could have appeared to influence the work reported in this paper.

Acknowledgements

RV *Sonne* cruises 187 and 220 were funded by the German Ministry of Science and Education (grant no. 03G0187 and 03G0220B). The Radiology section of the Medical Care Centre (Prüner Gang) in Kiel (Germany) generously provided access to their equipment. Achim Reisdorf (Basel) drew most of the figures. Constructive reviews by W. Szczuciński (Posnan, Poland) and M. Wiesner (Hamburg, Germany) were of great use to improve the paper. A.W. received funds from the Swiss National Foundation (SNF grant nos. 200021-112128 and 200020_140217/1). A.S. and D.U. were financially supported by the German Science Foundation (grant no. STA 401-10 to K.S.). All these contributions are gratefully acknowledged.

References

Alqahtani, F.A., Johnson, H.D., Jackson, C.-A.-L., Som, M.R.B., 2015. Nature, origin and evolution of a Late Pleistocene incised valley-fill, Sunda Shelf Southeast Asia. Sedimentology 62, 1198–1232.

Arz, H.W., Pätzold, J., Wefer, G., 1998. Correlated millennial-scale changes in surface hydrography and terrigenous sediment yield inferred from last-glacial marine deposits off Northeastern Brazil. Quat. Res. 50, 157–166.

Binh, D.V., Kantoush, S., Sumi, T., 2020. Changes to long-term discharge and sediment loads in the Vietnamese Mekong Delta caused by upstream dams. Geomorphology 353, 107011 (14 p.).

Blum, M., Martin, J., Milliken, K., Garvin, M., 2013. Paleovalley systems: Insights from Quaternary analogs and experiments. Earth Sci. Rev. 116, 128–169.

Borges, J., Huh, Y., 2007. Petrography and chemistry of the bed sediments of the Red River in China and Vietnam: Provenance and chemical weathering. Sed. Geol. 194, 155–168.

Boyd, R., Dalrymple, R.W., Zaitlin, B.A., 2006. Estuary and incised valley facies models. In: Posamentier, H.W., Walker, R.G. (Eds.), Facies Models Revisited. SEPM (Society for Sedimentary Geology) Special Publication 84, 171–234.

Bridge, J.S., 2003. Rivers and Floodplains. Blackwell, Oxford, p. 491.

Bui, V.D., Stattegger, K., Unverricht, D., Phung, V.P., Nguyen, T.T., 2013. Late Pleistocene-Holocene seismic stratigraphy of the Southeast Vietnam Shelf. Global Planet. Change 110, 156–169.

Casteltort, S., van den Driessche, J., 2003. How plausible are high-frequency sediment supply-driven cycles in the stratigraphic record? Sed. Geol. 157, 3–13.

Calvert, S.E., Pedersen, T.F., 2007. Elemental proxies for palaeoclimatic and palaeoceanographic variability in marine sediments: interpretation and application. In: C. Hillaire-Marcel, C., de Vernal, A. (Eds.), Proxies in Late Cenozoic Paleoceanography. Developments in Marine Geology 1. Elsevier, Amsterdam, pp. 567–644.

Carlin, J.A., Dellapenna, T.M., Strom, K., Noll, C.J.I., 2015. The influence of a salt wedge intrusion on fluvial suspended sediment and the implications for sediment transport to the adjacent coastal ocean: A study of the lower Brazos River TX, USA. Mar. Geol. 359, 134–147.

Clift, P.D., 2006. Controls on the erosion of Cenozoic Asia and the flux of clastic sediment to the ocean. Earth Planet. Sci. Lett. 241, 571–580.

Clift, P., Lee, G.H., Duc, N.A., Barckhausen, U., van Long, H., Zhen, S., 2008. Seismic reflection evidence for a Dangerous Grounds miniplate: No extrusion origin for the South China Sea. Tectonics 27, TC3008 (16 p.).

Coleman, J., 1969. Bottom sediments of the Gulf of Tonkin. Internal Report No. 69-32, Access No. AD 0855887. Naval Oceanographic Office, Washington. 24 p.

Constantine, J. A., T., D., Ahmed, J., Legleiter, C., Lazarus, E. D., 2014. Sediment supply as a driver of river meandering and floodplain evolution in the Amazon Basin. Nature Geoscience 7, 899–903.

Curtis, C.D., Coleman, M.L., 1986. Controls on the precipitation of early diagenetic calcite, dolomite, and siderite concretions in complex depositional sequences. In: Gautier, D.L. (Ed.), Relationships of Organic Matter and Mineral Diagenesis. SEPM Special Publication 38, 23–33.

Dalrymple, R.W., Mackay, D.A., Ichaso, A.A., Choi, K.S., 2012. Processes, morphodynamics, and facies of tide-dominated estuaries. In: Davis, R.A., Jr., Dalrymple; R.W. (Eds.), Principles of Tidal Sedimentology. Springer, Dordrecht, Heidelberg, pp. 79–107.

Darmadi, Y., Willis, B.J., Dorobek, S.L., 2007. Three-dimensional seismic architecture of fluvial sequeneces on the low-gradient Sunda Shelf, offshore Indonesia. J. Sediment. Res. 77, 225–238.

Dashtgard, S.E., Venditti, J.G., Hill, P.R., Sisulak, C.F., Johnson, S.M., La Croix, A.D., 2012. Sedimentation across the tidal-fluvial transition in the lower Fraser River. Canada. Sedimentary Record 10 (4), 4–9.

Dung, B.V., Stattegger, K., Unverricht, D., Phach, P.V., Thanh, N.T., 2013. Late Pleistocene-Holocene seismic stratigraphy of the Southeast Vietnam Shelf. Global Planet. Change 110, 156–169.

Emery, D., Myers, K., 1996. Sequence Stratigraphy. Blackwell, Oxford, p. 297.

Fagherazzi, S., Howard, A.D., Wiberg, P.L., 2004. Modeling fluvial erosion and deposition on continental shelves during sea level cycles. J. Geophys. Res. 109. F03010 (16 p.).

Fraser, G.S., 1994. Sequences and sequence boundaries in glacial sluiceways beyond glacial margins. In: Dalrymple, R.W., Boyd, R., Zaitlin, B.A. (Eds.), Incised Valley Systems: Origin and Sedimentary Sequences. SEPM (Society for Sedimentary Geology) Special Publication 51, 337–351.

Funabaki, A., Haruyama, S., Nguyen, V.O., Pham, V.H., Dinh, H.T., 2007. Holocene delta plain development in the Song Hong (Red River) delta. Vietnam. Journal of Asian Earth Sciences 30, 518–529.

Fyhn, M.B.W., Phach, P.V., 2015. Late Neogene structural inversion around the northern Gulf of Tonkin, Vietnam: Effects of right-lateral displacement across the Red River fault zone. Tectonics 33, 290–312.

Gingras, M.K., MacEachern, J.A., Dashtgard, S.E., Zonneveld, J.-P., Schoengut, J., Ranger, M.J., Pemberton, S.G., 2012. Estuaries. In: Knaust, D., Bromley, R.G. (Eds.), Trace Fossils as Indicators of Sedimentary Environments. Developments in Sedimentology, 64. Elsevier, Amsterdam, pp. 463–505.

Gong, Z.S., Huang, L.F., Chen, P.H., 2011. Neotectonic controls on petroleum accumulations, offshore China. J. Pet. Geol 34, 5–28.

Grant, J.A., Schreiber, R., 1990. Modern swathe sounding and sub-bottom profiling technology for research applications: the Atlas hydrosweep and parasound systems. Mar. Geophys. Res. 12, 9–19.

Gugliotta, M., Saito, Y., 2019. Matching trends in channel width, sinuosity, and depth along the fluvial to marine transition zone of tide-dominated river deltas: The need for a revision of depositional and hydraulic models. Earth Sci. Rev. 191, 93–113.

Gugliotta, M., Saito, Y., Nguyen, V.L., Ta, T.K.O., Nakashima, R., Tamura, T., Uehara, K., Katsuki, K., Yamamoto, S., 2017. Process regime, salinity, morphological, and sedimentary trends along the fluvial to marine transition zone of the mixed-energy Mekong River delta. Vietnam. Continental Shelf Research 147, 7–26.

Hanebuth, T.J.J., Stattegger, K., 2003. The stratigraphic evolution of the Sunda Shelf during the past fifty thousand years. In: Sidi, F.H., Nummedal, D., Imbert, P., Darman, H., Posamentier, H.W. (Eds.), Tropical Deltas of Southeast Asia - Sedimentology, Stratigraphy, and Petroleum Geology. SEPM (Society for Sedimentary Geology) Special Publication 76, 189–200.

Hanebuth, T.J.J., Stattegger, K., Saito, Y., 2002. The stratigraphic architecture of the central Sunda Shelf (SE Asia) recorded by shallow-seismic surveying. Geo-Mar. Lett. 22, 86–94.

Hanebuth, T.J.J., Stattegger, K., Bojanowski, A., 2009. Termination of the Last Glacial Maximum sea-level lowstand: The Sunda-Shelf data revisited. Global Planet. Change 66, 76–84.

Helland-Hansen, W., Hampson, G.J., 2009. Trajectory analysis: concepts and applications. Basin Res. 21, 454–483.
Hoekstra, P., van Weering, T.C.E.E., 2007. Morphodynamics of the Red River Delta, Vietnam (Special Issue). Journal of Asian Earth Sciences 29, 505–584.
Hori, K., Tanabe, S., Saito, Y., Haruyama, S., Nguyen, V., Kitamura, A., 2004. Delta initiation and Holocene sea-level change: example from the Song Hong (Red River) delta. Vietnam. Sedimentary Geology 164, 237–249.
Jagodziński, R., Sternal, B., Stattegger, K., Szczuciński, W., 2020. Sediment distribution and provenance on the continental shelf off the Mekong River, SE Vietnam: Insights from heavy mineral analysis. J. Asian Earth Sci. 196, 104357 (16 p.).
Janocko, M., Nemec, W., Henriksen, S., Warchol, M., 2013. The diversity of deep-water sinuous channel belts and slope valley-fill complexes. Mar. Pet. Geol. 41, 7–34.
Kineke, G.C., Sternberg, R.W., Trowbridge, J.H., Geyer, W.R., 1996. Fluid-mud processes on the Amazon continental shelf. Continental Shelf Research 16, 667–696.
Liu, Z.F., Zhao, Y.L., Ri, J.R., Colin, C., 2007. Late Quaternary clay minerals off Middle Vietnam in the western South China Sea: Implications for source analysis and East Asian monsoon evolution. Sci. China, Ser. D Earth Sci. 50, 1674–1684.
Loget, N., van den Driessche, J., 2009. Wave train model for knickpoint migration. Geomorphology 106, 376–382.
Lu, X.X., Siew, R.Y., 2006. Water discharge and sediment flux changes over the past decades in the Lower Mekong River: possible impacts of the Chinese dams. Hydrol. Earth Syst. Sci. 10, 181–195.
Ma, C.C., Nguyen, H.D., Le, D.N., Pham, H.L., 2004. Geological and mineralogical map of the Mekong delta, 1:500'000. In: Nguyen, H.D. (Ed.). Ministery of Natural Resources and Environment, Department of Geology and Minerals of Vietnam, Ho Chi Minh City (in Vietnamese).
MacEachern, J., Pemberton, S.G., Bann, K.L., Gingras, M.K., 2009. Departures from the archetypical ichnofacies: Effective recognition of physico-chemical stresses in the rock record. In: MacEachern, J.A., Bann, K.L., Gingras, M.K., Pemberton, S.G. (Eds.), Applied Ichnology (Revised Edition). SEPM Short Course Notes 51, 65–93.
Mathers, S., Zalasiewicz, J., 1999. Holocene sedimentary architecture of the Red River Delta. Vietnam. Journal of Coastal Research 15, 314–325.
Mattheus, C.R., Rodriguez, A.B., 2011. Controls on late Quaternary incised-valley dimension along passive margins evaluated using empirical data. Sedimentology 58, 1113–1137.
Menier, D., Reynaud, J.-Y., Proust, J.-N., Guillocheau, F., Guennoc, P., Bonnet, S., Tessier, B., Goubert, E., 2006. Basement control on shaping and infilling of valleys incised at the southern coast of Brittany, France. In: Dalrymple, R.W., Leckie, D.A., Tillman, R.W. (Eds.), Incised Valleys in Space and Time, 85. SEPM (Society for Sedimentary Geology) Special Publication, pp. 37–55.
Miall, A.D., 1996. The Geology of Fluvial Deposits. Springer, Berlin, Heidelberg, New York, p. 582.
Miall, A., 2010. Alluvial Deposits. In: James, N.P., Dalrymple, R.W. (Eds.), Facies Models 4. GEOtext, 6. St. John's, Geological Association of Canada, pp. 105–137.
Miall, A.D., 2011. Architecture and sequence stratigraphy of Pleistocene fluvial systems in the Malay Basin, based on seismic time-slice analysis. Am. Assoc. Pet. Geol. Bull. 86, 1201–1216.
Milliman, J.D., Meade, R.H., 1983. World-wide delivery of river sediment to the oceans. J. Geol. 91, 1–21.
Morley, C.K., 2002. A tectonic model for the Tertiary evolution of strike-slip faults and rift basins in SE Asia. Tectonophysics 347, 189–215.
Mozley, P.S., 1989. Relation between depositional environment and the elemental composition of early diagenetic siderite. Geology 17, 704–706.
Muto, T., Swenson, J.B., 2005. Large-scale fluvial grade as a non-equilibrium state in linked depositional systems: Theory and experiment. Journal of Geophysical Reseach F 110, F03002.
Nguyen, A.D., Savenije, H.H.G., Pham, D.N., Tang, D.T., 2008. Using salt intrusion measurements to determine the freshwater discharge distribution over the branches of a multi-channel estuary: The Mekong Delta case. Estuar. Coast. Shelf Sci. 77, 433–445.
Niino, H., Emery, K.O., 1961. Sediments of shallow portions of East China Sea and South China Sea. Geol. Soc. Am. Bull. 72, 731–762.
Phillips, J.D., Slattery, M.C., 2008. Antecedent alluvial morphology and sea-level controls on form-process transition zones in the lower Trinity River, Texas. River Res. Appl. 24, 293–309.
Plint, A.G., Wadsworth, J.A., 2006. Delta-plain paleodrainage patterns reflect small-scale fault movment and subtle forebulge uplift: Upper Cretaceous Dunvegan Formation, Western Canada Foreland Basin. In: Dalrymple, R.W., Leckie, D.A., Tillman, R.W. (Eds.), Incised Valleys in Space and Time. SEPM (Society for Sedimentary Geology) Special Publication 85, 219–237.
Portela, L.I., Ramos, S., Teixeira, A.T., 2013. Effects of salinity on the settling velocity of fine sediments of a habour basin. J. Coastal Res. 65, 1188–1193.
Postma, D., 1982. Pyrite and siderite formation in brackish and freshwater swamp sediments. Am. J. Sci. 282, 1151–1183.
Reijenstein, H.M., Posamentier, H.W., Bhattacharya, J.P., 2011. Seismic geomorphology and high-resolution seismic stratigraphy of inner-shelf fluvial, estuarine, deltaic and marine sequences, Gulf of Thailand. Am. Assoc. Pet. Geol. Bull. 95, 1959–1990.
Richter, T.O., van der Gaast, S., Koster, B., Vaars, A., Gieles, R., de Stigter, H.C., de Haas, H., van Weering, T.C.E., 2006. The avaatech core scanner: Technical description and applications to NE Atlantic sediments. In: Rothwell R.G. (Ed.), New Ways of Looking at Sediment Core and Core Data. Geological Society London Special Publication 267, 39–50.
Rickard, D., Luther, G.W., III., 2007. Chemistry of iron sulfides. Chemical Reviews 107, 514–562.
Sathiamurthy, E., Rahman, M.M., 2017. Late Quaternary paleo fluvial system research of Sunda Shelf: A Review. Bulletin of the Geological Society of Malaysia 64, 81–92.
Schimanski, A., Stattegger, K., 2005. Deglacial and Holocene evolution of the Vietnam shelf: stratigraphy, sediments and sea-level change. Mar. Geol. 214, 365–387.
Schumm, S.A., 1981. Evolution and response of the fluvial system, sedimentologic implications. In: Ethridge, F.G., Flores, R.M. (Eds.), Recent and Ancient Nonmarine Depositional Environments – Models for Exploration. SEPM (Society for Sedimentary Geology) Special Publication 31, 19–29.
Schumm, S.A., 1993. River response to base level change: implications for sequence stratigraphy. J. Geol. 101, 279–294.
Simms, A., Anderson, J.B., Taha, Z.P., Rodriguez, A.B., 2006. Overfilled versus underfilled incised valleys: Examples from the Quaternary Gulf of Mexico. In: Dalrymple, R.W., Leckie, D.A., Tillman, R.W. (Eds.), Incised Valleys in Space and Time. SEPM (Society for Sedimentary Geology) Special Publication 85, 117–139.
Stattegger, K., Tjallingii, R., Saito, Y., Michelli, M., Trung Thanh, N., Wetzel, A., 2013. Mid- to late Holocene sea-level reconstruction of Southeast Vietnam using beachrock and beach-ridge deposits. Global Planet. Change 110, 214–222.
Strong, N., Paola, C., 2008. Valleys that never were: Time surfaces versus stratigraphic surfaces. J. Sediment. Res. 78, 579–593.
Sutherland, B.R., Barrett, K.J., Gingras, M.K., 2015. Clay settling in fresh and salt water. Environ. Fluid Mech. 15, 147–160.
Szczuciński, W., Jagodziński, R., Hanebuth, T.J.J., Stattegger, K., Wetzel, A., Mitręga, M., Unverricht, D., Van Phach, P., 2013. Modern sedimentation and sediment dispersal pattern on the continental shelf off the Mekong River delta, South China Sea. Global Planet. Change 110, 195–213.
Tamura, T., Saito, Y., Sieng, S., ben, B., Kong, M., Sim, I., Choup, S., Akiba, F., 2009. Initiation of the Mekong River delta at 8 ka: evidence from the sedimentary succession in the Cambodia lowland. Quaternary Science Reviews 28, 327–344.
Tanabe, S., Saito, Y., Vu, Q.L., Hanebuth, T.J.J., Ngo, Q.L., Kitamura, A., 2006. Holocene evolution of the Song Hong (Red River) delta system, northern Vietnam. Sed. Geol. 187, 29–61.
Tanabe, S., Ta, T.K.O., Nguyen, V.L., Tateishi, M., Kobayashi, I., Saito, Y., 2003. Delta evolution model inferred from the Holocene Mekong delta, southern Vietnam. In: Sidi, F.H., Nummendal, D., Imbert, P., Darman, H., Posamentier, H.W. (Eds.), Tropical Deltas of Southeast Asia – Sedimentology, Stratigraphy, and Petroleum Geology. SEPM (Society for Sedimentary Geology) Special Publication 76, 175–188.
Tjallingii, R., 2007. Application and quality of XRF core scanning in reconstructing late Pleistocene NW African continental margin sedimentation and paleoclimate variations. PhD Thesis Thesis. Universität Bremen, p. 114 p..
Tjallingii, R., Stattegger, K., Wetzel, A., Van Pach, P., 2010. Infilling and flooding of the Mekong River incised-valley system during deglacial sea-level rise. Quat. Sci. Rev. 29, 1432–1444.
Tjallingii, R., Stattegger, K., Stocchi, P., Saito, Y., Wetzel, A., 2014. Rapid flooding of the southern Vietnam shelf during the early to mid-Holocene. J. Quat. Sci. 29, 581–588.
Tomczak, M., Godfrey, J.S., 1994. Regional Oceanography. Pergamon, London, p. 422.
Twidale, C.R., 2004. River patterns and their meaning. Earth Sci. Rev. 67, 159–208.
Unverricht, D., Nguyen, T.C., Heinrich, C., Szczuciński, W., Lahajnar, N., Stattegger, K., 2014. Suspended sediment dynamics during the inter-monsoon season in the subaqueous Mekong Delta and adjacent shelf, southern Vietnam. J. Asian Earth Sci. 79, 509–519.
van Maren, D.S., 2007. Water and sediment dynamics in the Red River mouth and adjacent coastal zone. J. Asian Earth Sci. 29, 508–522.
van Wagoner, J.C., Posamentier, H.W., Mitchum, R.M., Vail, P.R., Sarg, J.F., Loutit, T.S., Hardenbol, J., 1988. An overview of the fundamentals of sequence stratigraphy and key definitions. In: Wilgus, C.K., Hastings, B.S., Kendall, C.G.S.C., Posamentier, H. W., Ross, C., van Wagoner, J.C. (Eds.), Sea-Level Changes: An Integrated Approach. Society of Economic Palaeontologists and Mineralogists Special Publication 42, 39–45.
van Wagoner, J.C., Mitchum, R.M., Campion, K.M., Rahmanian, V.D., 1990. Siliciclastic Sequence Stratigraphy in Well Logs, Cores, and Outcrops. American Association of Petroleum Geologists, Methods in Exploration Series 7, 55 p.
Voris, H.K., 2000. Maps of Pleistocene sea levels in Southeast Asia: shorelines, river systems and time durations. J. Biogeogr. 27, 1153–1167.
Waelbroeck, C., Labeyrie, L., Michel, E., Duplessy, J.C., McManus, J.F., Lambeck, K., Balbon, E., Labracherier, M., 2002. Sea-level and deep water temperature change derived from benthic foraminifera isotopic record. Quat. Sci. Rev. 21, 295–305.
Wang, P. and Li, Q., 2009. The South China Sea. Paleoceanography and Sedimentology. Developments in Paleoenvironmental Research, 13. Springer, Berlin, Heidelberg, New York, 506 p.
Wang, R., Colombera, L., Mountney, N.P., 2019. Geological controls on the geometry of incised-valley fills: Insights from a global dataset of late-Quaternary examples. Sedimentology 66, 2134–2168.
Wang, L., Sarnthein, M., Erlenkeuser, H., Grimalt, J., Grootes, P., Heilig, S., Ivanova, E., Kienast, M., Pelejero, C., Pflaumann, U., 1999. East Asian monsoon climate during the Late Pleistocene: high-resolution sediment records from the South China Sea. Mar. Geol. 156, 245–284.
Weltje, G.J., Tjallingii, R., 2008. Calibration of XRF core scanners for quantitative geochemical logging of sediment cores: theory and application. Earth Planet. Sci. Lett. 274, 423–438.
Werner, F., 1967. Röntgen-Radiographie zur Untersuchung von Sedimentstrukturen. Umschau 16, 532.
Wetzel, A., Unverricht, D., 2020. Sediment dynamics of estuarine Holocene incised-valley fill deposits recorded by *Siphonichnus* (ancient Red River, Gulf of Tonkin). Palaeogeogr. Palaeoclimatol. Palaeoecol. 560, 110041 (13 p.).
Wetzel, A., Tjallingii, R., Stattegger, K., 2010. *Gyrolithes* in Holocene estuarine incised-valley fill deposits, offshore southern Vietnam. Palaios 25, 239–246.
Wetzel, A., Williams, C., Kassens, H., Leger, G., Auroux, C., 1990. Comparison between laboratory-determined physical properties and downhole measurements in outer

Bengal Fan deposits. In: Cochran, J.R., Stow, D.A.V., Scientific Party (Eds.). Proceedings of the Ocean Drilling Program, Scientific Results 116, 369–374.

Weber, N., Chaumillon, E., Tesson, M., Garlan, T., 2004. Architecture and morphology of the outer segment of a mixed tide and wave-dominated-incised valley, revealed by HR seismic reflection profiling: the paleo-Charente River France. Marine Geol. 207, 17–38.

Wetzel, A., Szczygielski, A., Unverricht, D., Stattegger, K., 2017. Sedimentological and ichnological implications of rapid Holocene flooding of a gently sloping mud-dominated incised valley – an example from the Red River (Gulf of Tonkin). Sedimentology 64, 1173–1202.

Wiesner, M.G., Stattegger, K., Pohlmann, T., Chen, F., Heddaeus, A., Heyckendorff, K., Jechlitschek, H., Lahajnar, N., Liskow, I., Li, X., Liu, Z., Lorenc, S., Metzke, M., Müller, M., Peleo-Alampay, A., Schönke, M., Schwarzer, K., Szczygielski, A., Steen, E., Unverricht, D., Wangh, X., Welsch, A., Wetzel, A., Zhao, Y., 2012. Cruise Report RV Sonne 220 – Land-Ocean-Atmosphere Interactions in the Gulf of Tonkin. Institut für Geowissenschaften der Christian-Albrechts-Universität zu Kiel, 101 p.

Wiesner, M.G., Stattegger, K., Voß, M., Schwarzer, K., Pohlmann, T., Amann, T., Dombar, D., de Silva, L., Dippner, J., Do, H.C., Doan, N.H., Kiem, D.T., Freing, A., Grosse, J., Heidemann, U., Hein, H., Heyckendorf, K., Hung, V.P., Jagodziński, R., Kagelmacher, A., Lahajnar, N., Le, X.T., Liskow, I., Moisander, P., Montoya, J., Nguyen, B.M., Nguyen, D.C., Nguyen, H.H., Nguyen, K.V., Nguyen, N.L., Nguyen, T. T., Nguyen, V.T., Peinert, R., Peleo-Alampay, A., Schimanski, A., Steen, E., Stochel, T., Subramaniam, A., Szczuciński, W., Tran, V.C., Unverricht, D., Vo, V.L., Welsch, A., Wetzel, A., 2006. Cruise report RV Sonne 187 Vietnam. Land-Ocean-Atmosphere Interactions in the Coastal Zone of Vietnam. Berichte – Reports 23. Institut für Geowissenschaften der Christian-Albrechts-Universität zu Kiel, 99 p.

Wolanski, E., Nguyen, N.H., Dao, L.T., Nguyen, H.N., Nguyen, N.T., 1996. Fine-sediment dynamics in the Mekong River estuary. Estuaries, Coastal and Shelf Science 43, 565–582.

Zaitlin, B.A., Dalrymple, R.W., Boyd, R., 1994. The stratigraphic organization of incised-valley systems associated with relative sea-level change. In: Dalrymple, R.W., Boyd, R., Zaitlin, B.A. (Eds.), Incised-valley Systems: Origin and Sedimentary Sequences. SEPM (Society for Sedimentary Geology) Special Publication 51, 45–60.

Zhang, X., Lin, C.-M., Dalrymple, R.W., Gao, S., Li, Y.-L., 2014. Facies architecture and depositional model of a macrotidal incised-valley succession (Qiantang River estuary, eastern China), and differences from other macrotidal systems. Geol. Soc. Am. Bull. 126, 499–522.